Alexandria Engineering Journal (2014) 53, 275–280

Alexandria University

Alexandria Engineering Journal

www.elsevier.com/locate/aej
www.sciencedirect.com

ORIGINAL ARTICLE

Comparison of inviscid and viscous transonic flow field in VKI gas turbine blade cascade

S.A. Moshizi *, A. Madadi, M.J. Kermani

Department of Mechanical Engineering, Amirkabir University of Technology, Tehran 15875-4413, Iran

Received 8 August 2013; revised 3 March 2014; accepted 12 March 2014
Available online 3 April 2014

KEYWORDS

Gas turbine cascade;
Viscous flow;
Inviscid flow;
Turbulent flow;
Roe scheme;
Shock creation

Abstract In this paper, the viscous and inviscid flow fields of a gas turbine blade cascade are investigated. A two-dimensional CFD solver is developed to simulate the flow field through VKI blade cascade. A high resolution flux difference splitting scheme of Roe is applied to discretize the convective part of Navier–Stokes equations. Baldwin Lomax (BL) model is used to account for turbulent effects on the viscous flow field of the blade cascade. For validation of the code, the flow field was solved by Ansys Fluent commercial software. The flow solution was done by third order flux difference splitting scheme of Roe and k–ω turbulence model. The findings show that the high turbulent and the shock creation in the flow field, lead to the same results in viscous and inviscid flows. Also, the results show that the grid and solver's focus must be on the precise prediction of the shock effects, when the shock is occurred in the domain.

1. Introduction

Gas and steam turbines are widely used to generate power in the power generation industries, because they are capable of producing power in hundred of megawatts. The aerodynamic performance is a major factor for the turbine efficiency. Cascade tests have been implemented during the years to find out aerodynamic losses in turbomachines. The cascade results are used to validate flow computation programs and to further refine their accuracy in predicting flow phenomenon in turbomachines. Although the results from such tests are not as precise as the data obtained from the tests conducted on the operating turbomachine, cascade test provides a blade designer a more economical alternative to determine the aerodynamic efficiency of the blades under various operating conditions. In addition, these programs are able to predict losses reasonably well for subsonic flows. However, in transonic flow, shock-boundary layer interaction is evident and the structure of this interaction is complex and difficult to predict. Until significant progress is achieved in refining the available flow computation programs in the industries, cascade test is still an effective method to determine aerodynamic losses of turbomachines [1].

Based on the importance of cascade investigation, many researchers have been studied turbomachine cascades experimentally and numerically. Arts et al. [2] experimentally investigated the aerodynamic and thermal performance of

* Corresponding author. Tel.: +98 9363761760.
E-mail address: s.a.moshizi@aut.ac.ir (S.A. Moshizi).

Peer review under responsibility of Faculty of Engineering, Alexandria University.

Production and hosting by Elsevier

1110-0168 © 2014 Production and hosting by Elsevier B.V. on behalf of Faculty of Engineering, Alexandria University.
http://dx.doi.org/10.1016/j.aej.2014.03.007

Nomenclature

C_p	pressure coefficient
c	blade chord
P	static pressure
Re	Reynolds number
S	blade pitch
u_τ	friction velocity
u^+	non-dimensional velocity
y^+	non-dimensional normal distance
ϑ	kinematic viscosity
κ	von Karman constant
α	angle of attack
β	outlet flow angle
η	normal generalized direction
ξ	stream wise generalized direction
μ	viscosity

Subscripts

0	stagnation condition
1	parameter at blade inlet
2	parameter at blade outlet
ti	internal layer
to	external layer
x	derivative relative to x
y	derivative relative to y
tur	turbulent
∞	free stream

VKI (von Karman Institute) gas turbine blade cascade. They studied the various flow conditions, and discussed the effects of Mach number, Reynolds number and flow turbulence intensity on the aerodynamic and thermodynamic performance of the blade. Dennis et al. [3] investigated the optimal design of a two-dimensional blade cascade. They studied the VKI blade cascade compressible flow field using Navier–Stokes solver with unstructured grid and k–ε turbulent model. Also, performing a supersonic through-flow fan (STF) blade cascade, Chesnakas and Ng [4] showed that the leading edge radius is a major source of losses in STF blades. Their results reported that losses from the leading-edge bluntness are convected downstream into the blade wake and are difficult to distinguish from viscous losses. Shock losses account for 70–80% of the losses in the STF cascade.

In 1905, Ludwig Prandtl [5] assumed that for the fluids with small viscosities except near the solid surface, where the flow must satisfy the no-slip conditions, in all other areas of the flow field, the viscous forces can be ignored. Hence, in fluid flows near the body surfaces, a thin layer, called "Boundary Layer" would appear in which the viscosity effects are significant [6]. There is an extensive literature on the boundary layer flow, but we only refer to few recent studies [7–11]. Boundary layers in turbines are usually thin and an increase in Reynolds number of the flow leads to the layer get thinner. Since, at the inlet stage of a turbine the boundary layer is laminar; the friction loss from viscous interaction with the blade surface is low. The creation of boundary layer in turbomachines decreases its efficiency. Singhal and Spalding [12] presented a finite different scheme for calculating the steady two-dimensional flows in turbine blade cascade issues.

Recent investigations in the inviscid–viscous interaction as well as more complex Navier–Stokes codes are very encouraging, but still the transonic flow fields with strong imbedded shock waves and boundary layer separations create tremendous difficulties. Giles [13] showed that the strong shocks in a single-stage turbine produced 40% variation in the rotor blade lift. Paniagua et al. [14] investigated a detailed physical analysis of the stator–rotor interaction in a transonic turbine stage at three pressure ratios. They studied the behavior of shock-boundary layer interaction in the stator–rotor system. Graham and Kost [15] performed steady flow investigations on the shock-boundary layer interaction in a high turning transonic cascade with the help of schlieren flow visualization.

McBean et al. [16] used a parallel multiblock Navier–Stokes with k–ω turbulence model to solve the unsteady flow through an annular turbine cascade, the transonic Standards Test Case 4, Test 628. After determining the unsteady surface pressure and the aerodynamic damping, they compared them with the two- and three-dimensional inviscid, viscous simulations and experimental data. The results showed that the three-dimensionality of the cascade model and the presence of a boundary layer separation cause differences between stability predictions by the two- and three-dimensional computations.

Although a number of studies have been investigated flow field in the different blade cascades in inviscid and viscous flows, none of these has dealt with numerical losses due to boundary layer and shock formation. In the present work, the inviscid and viscous flow field through gas turbine blade cascade is analyzed with accurate computational fluid dynamics (CFD) calculations by means of Ansys Fluent software [17] and an in-house developed code. The outlet parameters of blade cascade are computed and studied for losses existence due to shock waves and boundary layer.

2. Governing equations

Full conservative Navier–Stokes equations for the viscous fluid and two-dimensional unsteady compressible flow considering no body force are used to simulate the flow filed between blades [18] as follows

$$\frac{\partial \boldsymbol{Q}}{\partial t}+\frac{\partial \boldsymbol{F}}{\partial x}+\frac{\partial \boldsymbol{G}}{\partial y}=\frac{\partial \boldsymbol{F}_{\boldsymbol{v}}}{\partial x}+\frac{\partial \boldsymbol{G}_{\boldsymbol{v}}}{\partial y} \tag{1}$$

where $\boldsymbol{Q}$ is the conservative vector, also $\boldsymbol{F}$ and $\boldsymbol{G}$ are the inviscid flux vectors. $\boldsymbol{F}_{\boldsymbol{v}}$ and $\boldsymbol{G}_{\boldsymbol{v}}$ are viscous flux vectors.

$$\boldsymbol{Q}=\begin{bmatrix}\rho\\ \rho u\\ \rho v\\ \rho e_t\end{bmatrix},\quad \boldsymbol{F}=\begin{bmatrix}\rho u\\ \rho u^2+P\\ \rho uv\\ \rho uh_t\end{bmatrix},\quad \boldsymbol{G}=\begin{bmatrix}\rho v\\ \rho uv\\ \rho v^2+P\\ \rho vh_t\end{bmatrix},$$
$$\boldsymbol{F}_{\boldsymbol{v}}=\begin{bmatrix}0\\ \tau_{xx}\\ \tau_{xy}\\ u\tau_{xx}+v\tau_{xy}-q_x\end{bmatrix},\quad \boldsymbol{G}_{\boldsymbol{v}}=\begin{bmatrix}0\\ \tau_{xy}\\ \tau_{yy}\\ u\tau_{xy}+v\tau_{yy}-q_y\end{bmatrix} \tag{2}$$

where τ_{xx}, τ_{xy}, and τ_{yy} are stress tensor components and q_x and q_y are conductive heat transfer in x- and y-directions, respectively. By using the chain derivative rule, Eq. (1) is transported from the physical space (x, y) to the computational space (ξ, η) as follows:

$$\frac{\partial \boldsymbol{Q}^*}{\partial t}+\frac{\partial \boldsymbol{F}^*}{\partial \xi}+\frac{\partial \boldsymbol{G}^*}{\partial \eta}=\frac{\partial \boldsymbol{F}_v^*}{\partial \xi}+\frac{\partial \boldsymbol{G}_v^*}{\partial \eta} \tag{3}$$

where

$$\begin{aligned}&\boldsymbol{Q}^*=\tfrac{Q}{J}, \quad \boldsymbol{F}^*=\tfrac{1}{J}(\xi_x\boldsymbol{F}+\xi_y\boldsymbol{G}), \quad \boldsymbol{G}^*=\tfrac{1}{J}(\eta_x\boldsymbol{F}+\eta_y\boldsymbol{G}),\\ &\boldsymbol{F}_v^*=\tfrac{1}{J}(\xi_x\boldsymbol{F}_v+\xi_y\boldsymbol{G}_v), \quad \boldsymbol{G}_v^*=\tfrac{1}{J}(\eta_x\boldsymbol{F}_v+\eta_y\boldsymbol{G}_v)\end{aligned} \tag{4}$$

where J is the jacobian of transformation and ξ_x, ξ_y, η_x, η_y are metrics of the transformation [18].

3. Flow field solution

In the present study, a developed code was used for solving the two-dimensional Navier–Stokes equations based on Roe's numerical upwind method [19]. The primitive variables have been extrapolated using the third-order MUSCL method [20,21]. The Baldwin–Lomax model [22] was used for turbulent flow simulation. The grids used in this paper were created by Gambit 2.3.16 commercial software which was transformed into the intended program by using a transformation code.

3.1. Baldwin–Lomax model

Baldwin–Lomax (BL) model [22] has been presented after the Cebeci–Smith model [23]. In this model the turbulent viscosity is computed as follows:

$$\mu_{tur}=\min(\mu_{ti},\mu_{to}) \tag{5}$$

where μ_{tur} is the turbulent viscosity, which is divided into one internal layer μ_{ti} and one external layer μ_{to}. In the internal layer, the turbulent viscosity is determined as follows:

$$\mu_{ti}=\rho l_s^2\omega \tag{6}$$

where l_s and ω are mixing length and flow vorticity, respectively, and are defined as the following equation:

$$l_s=\kappa y[1-\exp(-y^+/A^+)] \tag{7}$$

where y^+ is the non-dimensional distance from the wall:

$$y^+=\frac{\sqrt{\rho_w\tau_w}}{\mu_w}y \tag{8}$$

and,

$$\tau_w=\mu_w\frac{\partial V_{\tan}}{\partial y}\bigg]_{wall} \tag{9}$$

where V_{tan} is the tangent velocity to the wall. The flow vorticity ω is computed as follows:

$$\omega=\left|\frac{\partial u}{\partial y}-\frac{\partial v}{\partial x}\right| \tag{10}$$

In the external layer, the turbulent viscosity is computed as follows:

$$\mu_{to}=\rho KC_{cp}F_{wake}F_{Kleb}(y) \tag{11}$$

where

$$F_{wake}=\min\left\{y_{\max}F_{\max},\frac{C_{WK}y_{\max}u_{dif}^2}{F_{\max}}\right\} \tag{12}$$

and,

$$u_{diff}=(V_{tot})_{\max}-(V_{tot})_{\min} \tag{13}$$

where $V_{tot}=\sqrt{u^2+v^2}$ is the velocity magnitude. F is a function of the distance from the wall, and $F_{\max}$ is the maximum value of the F function. Also $y_{\max}$ is the distance from the wall where $F_{\max}$ occurs.

$$F(y)=y|\omega|[1-\exp(-y^+/A^+)] \tag{14}$$

and,

$$F_{Kleb}(y)=\left[1+5.5\left(\frac{C_{Kleb}y}{y_{\max}}\right)^6\right]^{-1} \tag{15}$$

F_{Kleb} is Klebanoof distance function, which is applied in order to decrease the turbulent viscosity toward zero in the far flow fields. The turbulent viscosity for the turbulent flows is calculated on the basis of Eq. (8), but for the laminar and transient flows, one can use the BL model as well:

$$\mu_{tur}=0 \quad \text{if} \quad (\mu_{tur})_{\max}<C_{MUTM}\mu_\infty \tag{16}$$

where μ_∞ is the laminar flow viscosity in the free stream. It should be mentioned that BL model's constants are summarized in Table 1.

4. Results and discussion

At first, to establish the accuracy of the inviscid solver, the flow field is solved for NACA65-410 compressor blade cascade. In Fig. 1, for instance, two blades of the compressor cascade have been illustrated. The total temperature, inlet total pressure, outlet static pressure and the inlet flow angle have been considered as 315 K, 118.6 kPa, 100 kPa and 30°, respectively. Fig. 2 shows a comparison of the numerical and experimental results for the pressure coefficient on the blade's surfaces. As it is shown, there is an acceptable agreement between the present numerical results and experimental results of Emery et al. [24].

In this paper, the VKI gas turbine blades have been studied [25,26]. To solve a blade cascade, four types of boundary conditions are presented: (1) wall, (2) periodic, (3) inlet and (4) outlet, as shown in Fig. 3. For the viscous flow, due to the no-slip condition, the velocity on the wall is set to zero. The pressure on the wall is extrapolated using the momentum equation. As the surface is assumed to be adiabatic, the temperature gradient on the wall will be zero. In the inlet boundary, the total pressure p_0, total temperature T_0 and inlet flow angle α, are given and static pressure is extrapolated from the interior. At the outlet boundary, the static pressure is given and the other variables are extrapolated from the flow field. In Table 2, the blades' characteristics and the inlet/outlet flow conditions are mentioned. The blades' geometry is shown in Fig. 4.

Table 1 Baldwin–Lomax model constants.

κ	A^+	K	C_{cp}	C_{Kleb}	C_{WK}	C_{MUTM}
0.4	26	0.0168	1.6	0.3	0.25	14.0

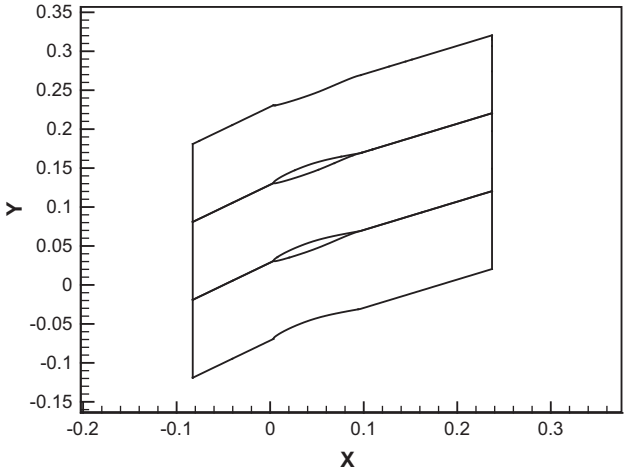

Figure 1 NACA65-410 compressor blade cascade for validating the inviscid flow solver.

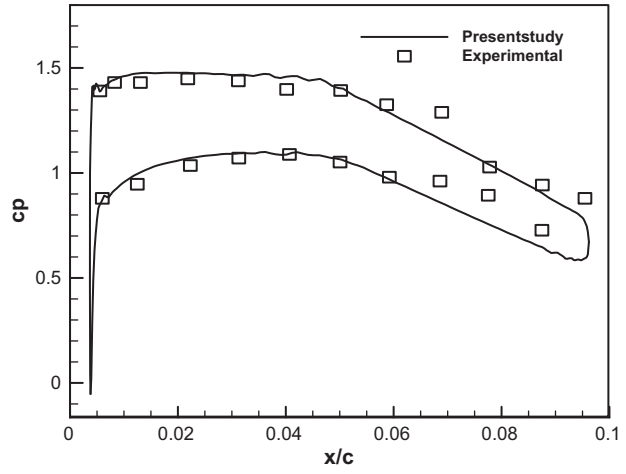

Figure 2 Comparing the results of inviscid solver and experimental data of Emery et al. [24] for NACA65-410 blade cascade.

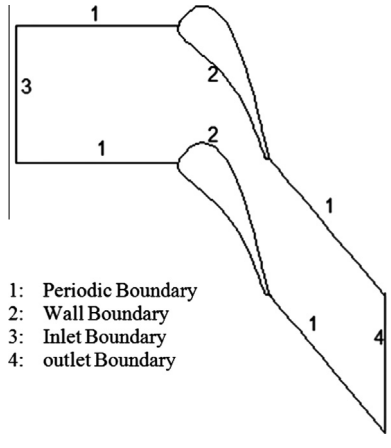

Figure 3 VKI turbine blade cascade boundary condition.

As the second test case, the flow field through the VKI turbine cascade is investigated. In Table 3, the numerical

Table 2 VKI blade characteristics and inlet/outlet conditions.

Parameters	P_{01} (kPa)	T_{01} (K)	P_{back} (kPa)	α (°)	S (m)
Values	430	278	101.3	1.9	1.51

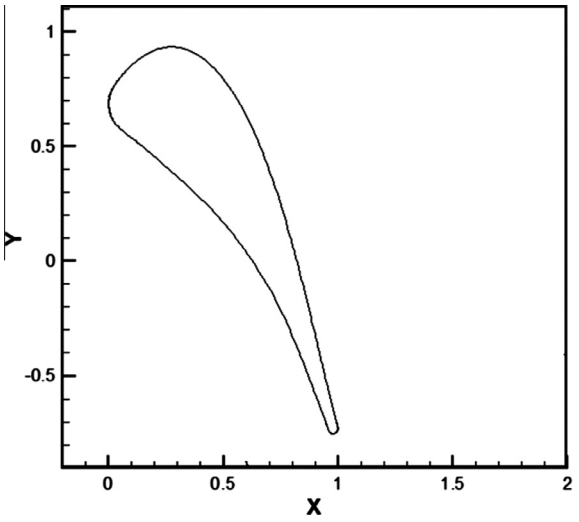

Figure 4 VKI turbine blade geometry.

Table 3 Comparisn between present study and Dennis et al. and fluent results.

VKI cascade	P_{02} (kPa)	β (°)	$\dot{m}$ (kg/m^3)
Dennis et al. [3]	–	−70	384
Present study	383.52	−70.1	395.4
Fluent solver	382.1	−69.64	396.6

results are compared with the results obtained by Dennis et al. [3]. The inlet/outlet boundary conditions are summarized in Table 2. The outlet flow angle is compatible with both Dennis's [3] and Fluent solver results. The blade cascade flow field has been solved using the third-order Roe's numerical method and k–ω turbulence model by Fluent software [17]. In addition, it is found that the flow rate results for both present numerical simulation and Dennis et al. [3] are in agreement with a difference less than 3%. In Figs. 5 and 6 the results of static pressure distribution on the blade surfaces are compared with the results of Fluent solver in both viscous and inviscid flows. A comparison of the flow field results for viscous and inviscid flows with similar inlet/outlet boundary conditions are given in Table 4. The boundary layer effect in the viscous flow decreases the available cross-sectional area of turbine cascade, hence the mass flow rate is decreased. Also, this cross-sectional reduction increases the outlet Mach number and decreases the outlet angle.

Shock is a form of physical discontinuity. Across the shock, static enthalpy, pressure and temperature will rise, whereas the stagnation enthalpy is unchanged. Fig. 7 indicates the computed Mach number contours using the Baldwin–Lomax turbulence model, including three important zones. When the flow passes through the two blades, the flow is choked at the

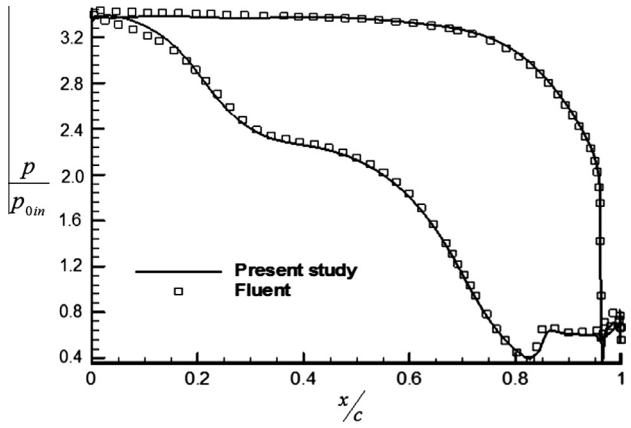

Figure 5 Static pressure distribution on the pressure and suction sides of the blade for viscous flow.

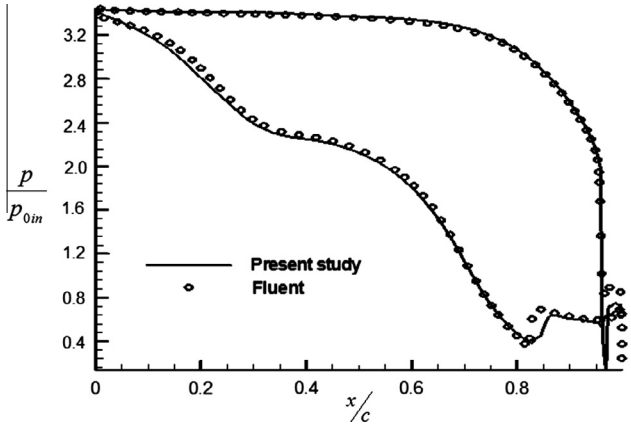

Figure 6 Static pressure distribution on the pressure and suction sides of the blade for inviscid flow.

cascade throat (zone 1). The fishtail shock formed near the trailing edge impinges on the suction surface of the subsequent blade and is reflected back as a shock (zone 2 in Fig. 7). The incident shock on the suction side causes a local boundary-layer separation as a result of pressure rise as shown in zone 3.

Because of shock and higher turbulence, effects of the boundary layer in the viscous flow are insignificant. Higher turbulence in the flow decreases the boundary layer thickness and will have an insignificant effect on the fluid flow. To ensure the accuracy, a comparison with Fluent software [17] is done as it is summarized in Table 4. Clearly, the same result has been obtained for two distinctive turbulence models; the

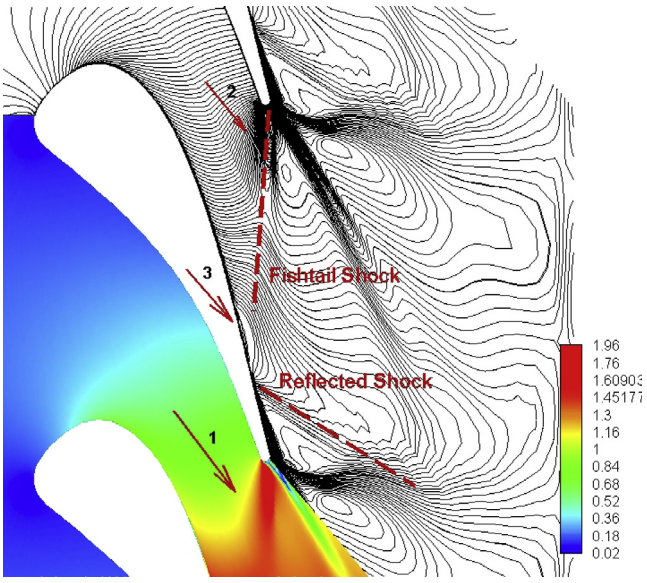

Figure 7 Mach number contours of the viscous flow through VKI gas turbine blade cascade.

fishtail shock and its interaction with blade boundary layer dominate the boundary layer losses. Hence, the results of viscous and inviscid flows which only differ on boundary layer losses are close together. Consequently, shock losses in the transonic turbine are much more than boundary layer losses. As it is obvious from p_{02}, it can be concluded that the pressure losses due to viscous flow are about 8 kPa.

5. Summary and conclusions

In this paper, the viscous and inviscid flow field solution of a gas turbine blade cascade is investigated. A two-dimensional CFD solver is developed to simulate the flow fields of the VKI blade cascade. For discretizing the convective part of Navier–Stokes equations, a high resolution flux difference splitting scheme of Roe is applied. Baldwin Lomax (BL) model is also used to account for turbulent effects on the viscous flow field of blade cascade. In addition to the code's validation with the experimental results, the flow field is solved by Fluent software. The turbulence model in Fluent software is considered as k–ω model. The results show the fishtail shock and its interaction with blade boundary layer dominate the boundary layer losses. In this condition, the reducted rate due to the fluid's viscosity is about 2% of the reduction out of shock creation. Therefore, one can say that when in the flow field, the shock

Table 4 Comparison between inviscid and viscous flow results.

VKI cascade	Inviscid		Viscous	
	Present study	Fluent software [17]	Present study	Fluent software [17]
P_{01} (kPa)	430	430	430	430
P_{02} (kPa)	391.71	390.55	383.51	382.14
M_2	1.51	1.47	1.5123	1.49
$\dot{m}$ (kg/m^3)	395.63	396.76	395.4	396.6
β	−70.13	−69.68	−70.1	−69.64

is occurred; the grid and solver's focus must be on the precise prediction of the shock effects.

References

[1] T.L. Chu, Effects of Mach Number and Flow Incidence on Aerodynamic Losses of Steam Turbine Blades, Virginia Polytechnic Institute and State University, 1999.

[2] T. Arts, M. Lambert de Rouvroit, A.W. Rutherford, Aero-Thermal Investigation of a Highly Loaded Transonic Linear Turbine Guide Vane Cascade, 174, Von Karman, 1990.

[3] B.H. Dennis, I.N. Egorov, Z.X. Han, G.S. Dulikravich, C. Poloni, Multi-objective optimization of turbomachinery cascades for minimum loss, maximum loading, and maximum gap-to-Chord ratio, Int. J. Turbo Jet Eng. 18 (2001) 10.

[4] C.J. Chesnakas, W.F. Ng, Supersonic through-flow fan blade cascade studies, J. Fluids Eng. 125 (5) (2003) 796–805.

[5] Ludwig Prandtl, Int. Commun. Heat Mass Transfer 12 (2) (1985) 111, Ludwig Prandtl 1875–1953.

[6] J. Arakeri, P.N. Shankar, Ludwig Prandtl and boundary layers in fluid flow, Reson 5 (12) (2000) 48–63.

[7] K.A. Hafez, O.A. Elsamni, K.Y. Zakaria, Numerical investigation of the fully developed turbulent flow over a moving wavy wall using k–ε turbulence model, Alexandria Eng. J. 50 (2) (2011) 145–162.

[8] A. Malvandi, F. Hedayati, D.D. Ganji, Thermodynamic optimization of fluid flow over an isothermal moving plate, Alexandria Eng. J. 52 (3) (2013) 277–283.

[9] A. Malvandi, D. Ganji Domairry, F. Hedayati, M. Kaffash Hossein, M. Jamshidi, Series solution of entropy generation toward an isothermal flat plate, Therm. Sci. 16 (5) (2012) 1289–1295.

[10] N. Bachok, A. Ishak, I. Pop, Boundary-layer flow of nanofluids over a moving surface in a flowing fluid, Int. J. Therm. Sci. 49 (9) (2010) 1663–1668.

[11] Y.M. Ahmed, Numerical simulation for the free surface flow around a complex ship hull form at different Froude numbers, Alexandria Eng. J. 50 (3) (2011) 229–235.

[12] A.K. Singhal, D.B. Spalding, A 2D Partially-Parabolic Procedure for Axial-Flow, 3807, Mechanical Engineering Department, Imperial College, 1976.

[13] M.B. Giles, Stator–rotor interaction in a transonic turbine, J. Propul. Power 6 (5) (1990) 621–627.

[14] G. Paniagua, T. Yasa, A.D. La Loma, L. Castillon, T. Coton, Unsteady strong shock interactions in a transonic turbine: experimental and numerical analysis, J. Propul. Power 24 (4) (2008) 722–731.

[15] C.G. Graham, F.H. Kost, Shock boundary layer interaction on high turning transonic turbine cascades, in: American Society of Mechanical Engineers Paper 79-GT-37, 1979.

[16] I. McBean, K. Hourigan, F. Liu, M. Thompson, Prediction of flutter of turbine blades in a transonic annular cascade, J. Fluids Eng. 127 (6) (2005) 1053–1058.

[17] ANSYS FLUENT User's Guide, Release 14.0, ANSYS Inc., November 2011.

[18] K.A. Hoffmann, S.T. Chiang, Computational Fluid Dynamics, Engineering Education System, 2000.

[19] P.L. Roe, Approximate Riemann solvers, parameter vectors, and difference schemes, J. Comput. Phys. 43 (2) (1981) 357–372.

[20] M. Kermani, E. Plett, Roe scheme in generalized coordinates. I – formulations, in: 39th Aerospace Sciences Meeting and Exhibit, American Institute of Aeronautics and Astronautics, 2001.

[21] M. Kermani, E. Plett, Roe scheme in generalized coordinates. II – application to inviscid and viscous flows, in: 39th Aerospace Sciences Meeting and Exhibit, American Institute of Aeronautics and Astronautics, 2001.

[22] B. Baldwin, H. Lomax, Thin-layer approximation and algebraic model for separated turbulent flows, in: 16th Aerospace Sciences Meeting, American Institute of Aeronautics and Astronautics, 1978.

[23] A.M.O. Smith, T. Cebeci, Numerical solution of the turbulent boundary layer equations, in: DAC 33735, 1967.

[24] J.C. Emery, L.J. Herrig, J.R. Erwin, A.R. Felix, Systematic Two Dimensional Cascade Tests of NACA 65-Series Compressor Blades at Low Speeds, 1368, 1958.

[25] F. Magagnato, B. Pritz, M. Gabi, Calculation of the VKI turbine blade with LES and DES, J. Therm. Sci. 16 (4) (2007) 321–327.

[26] F. Magagnato, J. Rachwalski, M. Gabi, numerical investigation of the VKI turbine blade by large eddy simulation, in: High Performance Computing in Science and Engineering' 05, Springer, Berlin Heidelberg, 2006, pp. 143–154.